Sensors and Actuators B 263 (2018) 94–102

Contents lists available at ScienceDirect

Sensors and Actuators B: Chemical

journal homepage: www.elsevier.com/locate/snb

AC phase sensing of graphene FETs for chemical vapors with fast recovery and minimal baseline drift

Huiliang Liu[a,b,*,1], Yumeng Liu[b,1], Yao Chu[a,b], Takeshi Hayasaka[b], Nirav Joshi[b], Yong Cui[b], Xiaohao Wang[a], Zheng You[a], Liwei Lin[a,b]

[a] Tsinghua-Berkeley Shenzhen Institute, Shenzhen, China
[b] Berkeley Sensor and Actuator Center, University of California, Berkeley, CA, USA

ARTICLE INFO

Article history:
Received 7 October 2017
Received in revised form 30 January 2018
Accepted 31 January 2018
Available online 3 February 2018

Keywords:
CVD graphene
Graphene FET
Chemical vapor
Room temperature
AC phase

ABSTRACT

This work utilizes an AC phase sensing approach of chemical vapors to achieve minimal baseline drift and fast recovery on graphene-based field effect transistors (FETs). Phase lag signals between channel resistance and gate voltage are detected with ultrafast recovery speed (~10 s) on defect-rich FETs made of chemical vapor deposition (CVD) graphene as the channel materials without surface functionalization at room temperature. The responses of the phase change upon exposure to water, methanol and ethanol vapors show at least ten times faster recovery speed than those of the conventional DC resistance measurements with minimal baseline drift, large dynamic range, and good stability. The effects of relative humidity on methanol and ethanol gas response properties are also studied. As such, the AC phase sensing scheme could open up a new class of research in gas sensors for improved sensing speed and baseline stability.

1. Introduction

Over the last decade, 2D materials have been widely studied for fundamental knowledge toward practical applications [1–3]. Materials such as graphene offer good characteristics as the base sensing structures, such as large surface to volume ratio, low electrical noise, low power consumption and process compatibility with integrated circuits [4,5]. Previously, researchers have reported the ability to realize molecule-level detections using a graphene FET for high sensitivity [6,7] as the emerging platform for chemical sensors [8–10]. The most common sensing mechanism is the DC resistance measurement which correlates with charge variations on the graphene surface due to external gas vapors [11,12]. The intrinsic slow process of the charge transfer and the adverse effect of defects on the graphene surface are two great challenges. For example, FET gas sensors made of CVD graphene with a film transfer process suffer from intrinsic slow dynamics in its interface trap states and defect-compensated charge transfer process [13–15]. As such, the recovery speed of CVD graphene sensors is slow, especially at room temperature. For example, the recovery of DC electrical conductance could take more than 1000 s [16] as vapors and charges are released from interface trap states/defects [17,18]. The resulting baseline drift has been a bottleneck for practical applications [19,20]. To address this issue, UV lights or heaters were previously used to help boost the recovery process [19,21,22], which inevitably increase the power consumption and system complexity.

The baseline drift could be reduced by using different electrical sensing schemes such as at high frequencies (100 kHz). Researchers have previously shown that the channel resistance of a graphene FET is sensitive to the change in the dielectric constant of the gas, rather than the adsorption reaction associated with charge transfer process [23]. In this present study, we report on an AC phase sensing approach in contrast to the conventional DC resistance sensing for minimal baseline drift and fast responses, as illustrated in Fig. 1a. To alleviate the problems stemming from the trap states and defects on graphene, this new scheme takes the advantages of the reversible and stable phase change signals instead of DC resistances. As shown in Fig. 1b, the phase lag between the channel resistance (point A and B between the source and drain of the FET) and the gate voltage is detected when an AC gate voltage at a moderate frequency is applied. Experimental results show that the phase lags of different vapors under various concentrations have fast recovery speeds in the ranges of 10 s, which are at least 10 times faster than those of DC resistance results with similar setups. Furthermore, the

* Corresponding author at: Tsinghua-Berkeley Shenzhen Institute, Shenzhen, China.
E-mail address: liuhl@berkeley.edu (H. Liu).
[1] Equal contribution as first author.

https://doi.org/10.1016/j.snb.2018.01.244
0925-4005/

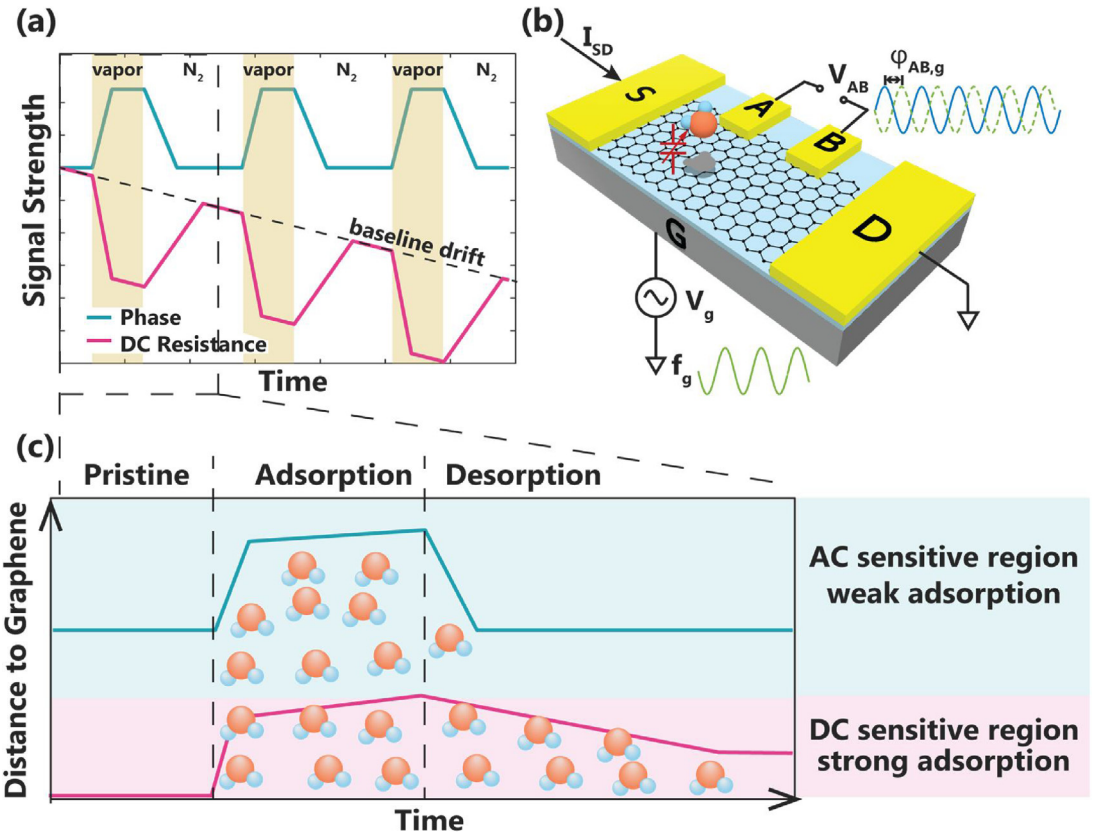

Fig. 1. (a) Schematic diagram illustrating the gas sensing performances between the phase lag detection scheme with minimal baseline drift and fast recovery speed as compared with the conventional DC resistance scheme on graphene-based gas sensors. (b) The setup of phase lag $\varphi_{AB,g}$ between V_{AB} and V_g on a CVD graphene FET sensor after the exposure to a specific chemical vapor. (c) The vapor adsorption and desorption on the graphene surface – the AC sensing scheme is targeting weakly adsorbed gases with a short distance from the graphene surface while the DC sensing scheme is targeting molecules very close to the graphene surface. This results in fast recovery for the AC sensing scheme.

dynamic response of the phase lag is reversible with large dynamic range while the DC resistance tests suffer from baseline drift problems. Fig. 1c illustrates the key differences between the AC and DC domain measurements, where the AC phase lag results are sensitive to the weak adsorption of vapor molecules above a distance to the graphene surface for fast gas adsorption and desorption processes, while the DC resistance results are sensitive to the strong adsorption and desorption process close to the graphene surface. These observations and analyses are explained by an analytical model with good match to the measurements.

2. Device and experiments

2.1. Preparation of graphene FET

The sensing material of our device is the monolayer graphene grown via the CVD method, which is available from Graphenea Inc. on top of a silicon die (10 mm × 10 mm) with 300 nm-thick, thermally grown SiO_2 on top. The following fabrication processes were carried out in the Marvell Nanofabrication Laboratory at UC Berkeley and also reported in details in our previous work [24]. First, four electrodes and contact pads (30 nm Pd/25 nm Au) were patterned on graphene by the lithography and lift-off process. Second, the graphene channel was patterned by the lithography and oxygen plasma (50 W, 7 s) etching process. Finally, the electrodes of graphene FET were connected to a custom designed test board by wire bonding. The optical microscopic picture and the SEM photo of the fabricated device are shown in Fig. 2a & b, respectively.

The fabricated device was purged with nitrogen overnight in the test chamber. Then, a milli-ampere level current was applied through the graphene channel for one minute as the thermal annealing process to remove surface contaminants [25]. The charge neutral point of the fabricated graphene FET was around 25 V (*p*-type doped) due to the unintentional doping of polymer residues during the device fabrication process. Therefore, results in this work were tested in the hole branch of graphene as the DC offset on the gate electrode was kept at 0 V.

2.2. Experimental setup

Fig. 3a illustrates the electrical configuration of the test setup, where the four-point probe method was used to avoid the influence of contact resistance in the measurement. An AC voltage was applied on the gate electrode with a frequency, f_g, ranging from 50 to 1000 Hz. A lock-in amplifier (SRS 860, Stanford Research Systems) was used to reduce the noise level at the source electrode with a reference of 20 kHz AC current (2 μA) through the graphene channel and a 1 MΩ resistor. The voltage between electrode A and B was measured by the lock-in amplifier. A data acquisition device (PicoScope 5242B) was used to collect V_{AB} and V_g simultaneously. With this setup, the phase lag between V_{AB} and V_g can be extracted by fast Fourier transform (FFT).

Fig. 3b illustrates the gas connections as all gas sensing measurements were carried out in a sealed nylon chamber (2 cm × 2 cm × 2 cm) with a waste gas treatment system. The concentration of a specific vapor was applied via the split-stream system with dry nitrogen (or dry air) and gas-saturated nitrogen

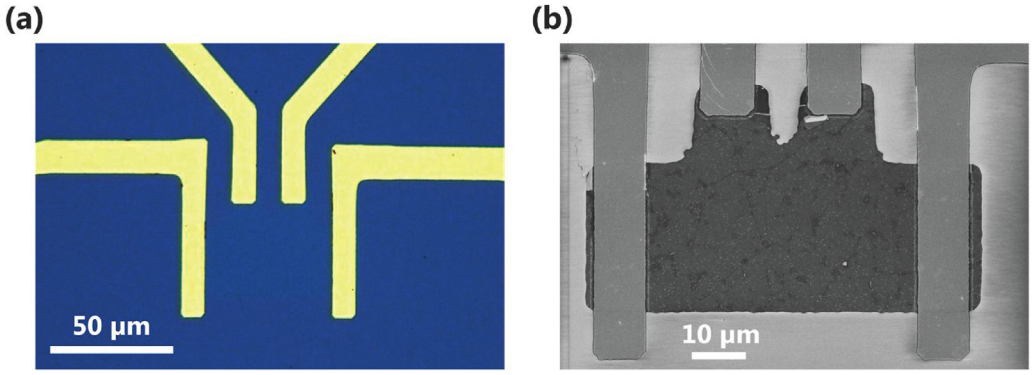

Fig. 2. (a) An optical photo and (b) SEM photo of a fabricated graphene FET sensor with scale bars of 50 μm and 10 μm, respectively.

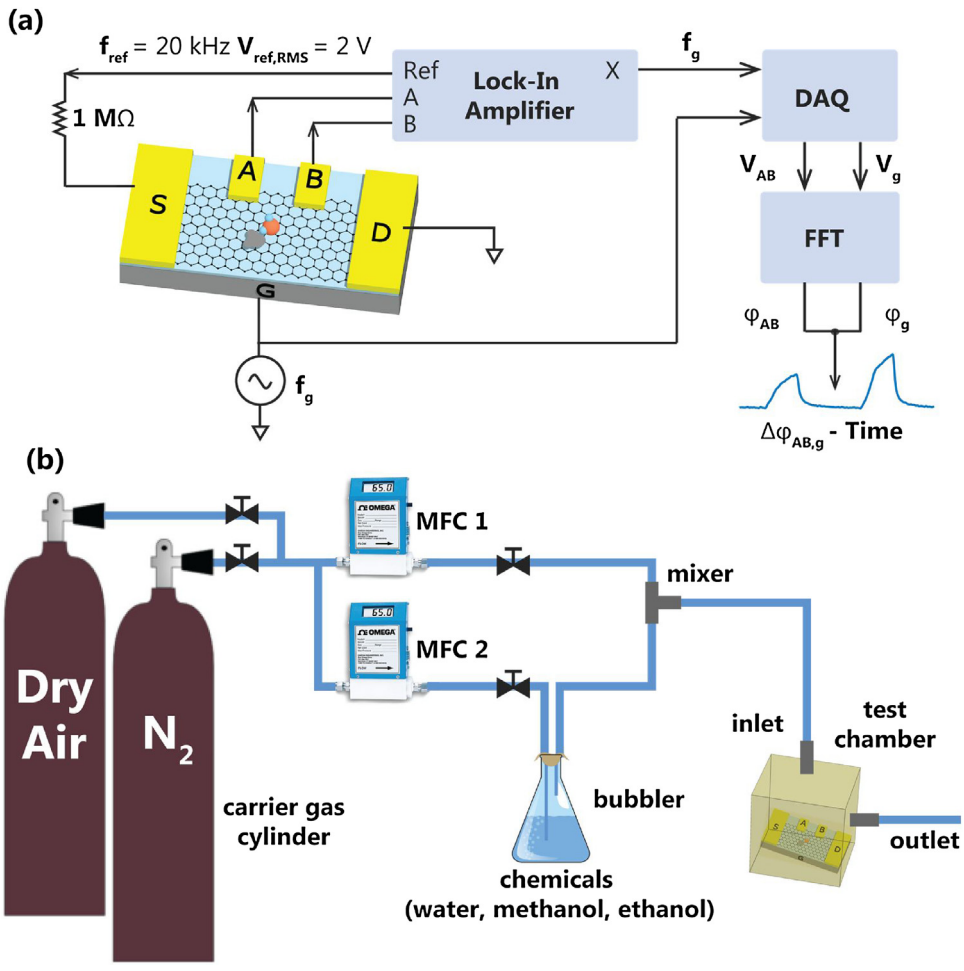

Fig. 3. Schematic diagram of the experimental setup for the phase lag detection on graphene showing (a) the electrical circuity and the flowchart for the data acquisition and processing, and (b) the gas routes of the test system.

(or air). The flow rates of both gas paths were regulated by mass flow controllers (Omega Engineering) and the total flow rate to the gas sensor was controlled at 200 sccm. To ensure no leakage around the seals, the flow rate at the outlet of the chamber was monitored by a mass flow meter (Omega Engineering). All experiments were carried out in a laboratory with general ventilation. The environmental temperature was 24 °C with fluctuations within 1 °C. The chemicals (DI water, anhydrous methanol, and anhydrous ethanol) were purchased from Sigma Aldrich, and inert gas (nitrogen) and dry air were purchased from Praxair Inc.

3. Results

The responses of the AC phase lag change $\Delta\varphi_{AB,g}$ and the changes of DC resistance $\Delta R/R_0$ are plotted under multiple sensing cycles of water, methanol, and ethanol vapors, respectively. Fig. 4a shows the inputs of vapor concentrations increasing from 10% to 90% stepwise and each cycle includes 40 s chemical vapor feeding followed with 160 s nitrogen purging. Fig. 4b shows the dynamic response of the phase lag at 1000 Hz, with minimal drift and the average recovery time is around 10 s. Fig. 4c shows the

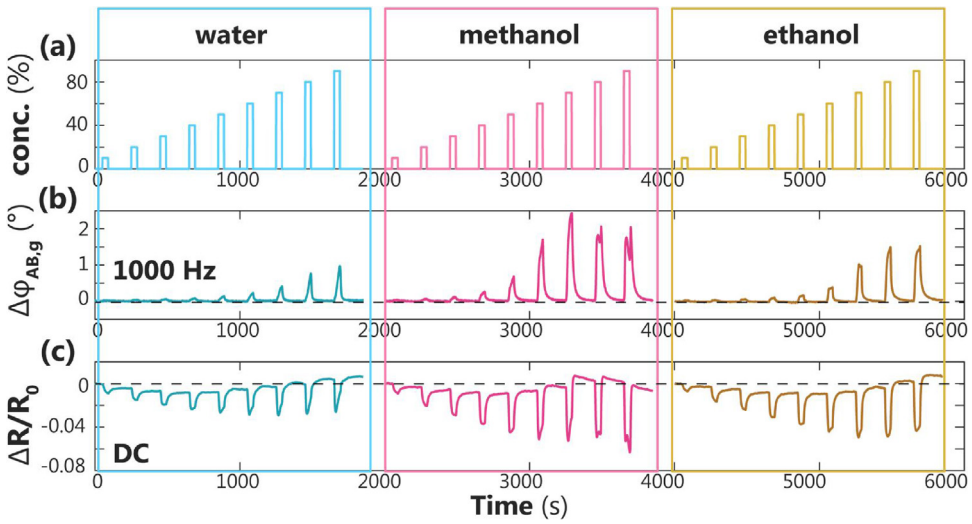

Fig. 4. Measurement results of three vapors (water, methanol, and ethanol) using the graphene FET sensor at room temperature. (a) Schematic of vapor concentrations. (b) Dynamic responses of the phase lag $\Delta\varphi_{AB,g}$ upon exposures to three different gases at a representative frequency of 1000 Hz. (c) Dynamic responses of the relative change of DC resistance $\Delta R/R_0$ upon exposures to different gases.

DC resistance changes which apparently have significant baseline drift issues as compared with phase lag responses. Furthermore, the average recovery time is larger than 100 s. In principle, the channel resistance decreases after the exposure to the *p*-type dopant molecules as the device is working in the hole branch of the graphene for all three *p*-type chemical vapors (water, methanol, and ethanol). After long-term exposures in high concentration vapors, the drop of the charge mobility in the graphene channel becomes significant to pull up the baseline resistance [26]. On the other hand, the phase lag responses in Fig. 4b are reversible upon the nitrogen purge process at room temperature as the phase lag response is immune to the strong adsorption gas reactions. For the three tested vapors, the amplitudes of DC resistance responses become saturated when the vapor concentrations are larger than 60% while the phase lag detections can still operate with up to 90% of water or methanol, and 80% of ethanol.

The dynamic responses of phase lag upon exposures to water, methanol and ethanol vapors in Fig. 5a, b, & c, respectively, at exemplary frequencies were studied at 50 Hz, 100 Hz, 500 Hz and 1000 Hz in nitrogen environment. It is observed that the amplitude of the phase lag change decreases for water vapor as the frequency increases, while the recovery responses at different frequencies have no big differences around 20 s. For methanol and ethanol, the amplitude of the phase lag change decreases and the recovery time reduces as the frequency increases in general. Specifically, the recovery time for 90% ethanol decreases from 80 to 30 s as the frequency increases from 50 Hz to 1000 Hz. These results imply that the recovery time can be reduced by using high frequency AC phase lag tests. The same experiment in nitrogen environment were carried out with the device stored in air atmosphere for three months to evaluate the stability of the gas sensors. The sensing results illustrate slight variations of 2%, 3% and 5% for water, methanol and ethanol vapors, respectively with good reproducibility (Fig. S1, Supplementary Information).

Further experiments were performed under different atmosphere conditions and the sensor responses at exemplary frequencies of 50 Hz, 100 Hz, 500 Hz and 1000 Hz upon exposures to water, methanol and ethanol vapors are shown in Fig. 5d, e, & f in the air environment. The resulting sensing patterns are similar to those responses in the nitrogen environment, which indicates our sensor is partially inert to the presence of the oxygen contents at room temperature. The performances are summarized and compared in Fig. 6. In Fig. 6a, b, & c, it is found that the response amplitudes in the air environment at 1000 Hz reduce *ca.* 5% when compared with those in the nitrogen environment and the average relative amplitude differences increase to *ca.* 10% as the frequency goes down to 50 Hz. The 90% gas sensing recovery time for water, methanol and ethanol with 90% concentration are summarized in Fig. 6d, e, & f. In general, the 90% gas sensing recovery time keeps at about 20 s for water vapor while for methanol and ethanol vapors, it reduces as the sensing frequency increases. Clearly, both the average response amplitude and recovery time decrease at higher frequency and there is a tradeoff between fast recovery speed and large sensing responses. To keep the 90% sensing recovery time to be within 40 s, the operating frequencies for water, methanol and ethanol vapors should be higher than 50 Hz, 1000 Hz and 500 Hz, respectively.

Representative sensing results of AC phase lag spectra upon exposures to three chemical vapors are recorded in the frequency versus time plot, including data for 60% (Fig. 7a–c) and 90% (Fig. 7d–f) gas concentrations of water, methanol, and ethanol, respectively. In these tests, the chemical vapors are injected to the system and nitrogen purge processes are conducted 50 s, and 90 s, respectively, after the start of the recording process. These phase lag spectra clearly highlight three important features. First, the recovery speed of the AC sensing scheme at high frequency is faster than those at low frequency as the dark blue color regions (no phase change) reappear faster during the nitrogen purge process. The nitrogen purge process helps the recovery and cleaning of the graphene surface, while weakly adsorbed gases (a short distance away from the graphene surface) can be removed easier than strongly adsorbed gases (close to the graphene surface). The conventional DC sensing signals are dominated by the desorption reaction for gases close to the graphene surface that is slow at room temperature. Second, the signal strength of the AC sensing scheme is smaller at high input frequency as the responsive gases are a short distance away from graphene surface. This can be considered as a tradeoff for the fast recovery speed by using the AC sensing scheme as it is more sensitive to the weakly adsorbed gases. Third, negative phase changes may occur under high concentrations of gases as observed in the case of 90% methanol under low frequency sensing in Fig. 5b. The negative values are not plotted in Fig. 7e and represented as zero phase change but the trend is also clearly observed. This is believed to be the accumulation of gas molecules at a short distance above graphene surface near saturated conditions that

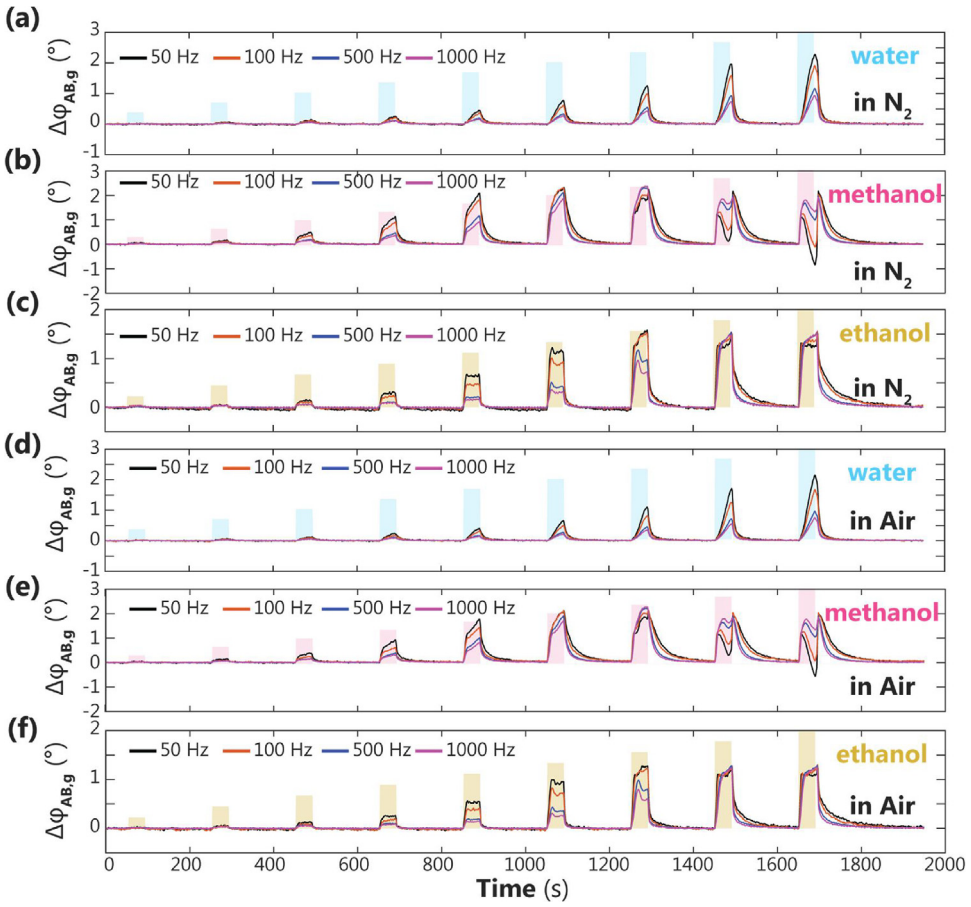

Fig. 5. Dynamic responses of phase lag changes at exemplary frequencies of 50 Hz, 100 Hz, 500 Hz, and 1000 Hz for (a) (d) water, (b) (e) methanol and (c) (f) ethanol vapors under various concentrations (from 10% to 90%) at room temperature. The shading color indicates the gas input and purging events in (a–c) nitrogen and (d–f) dry air environment.

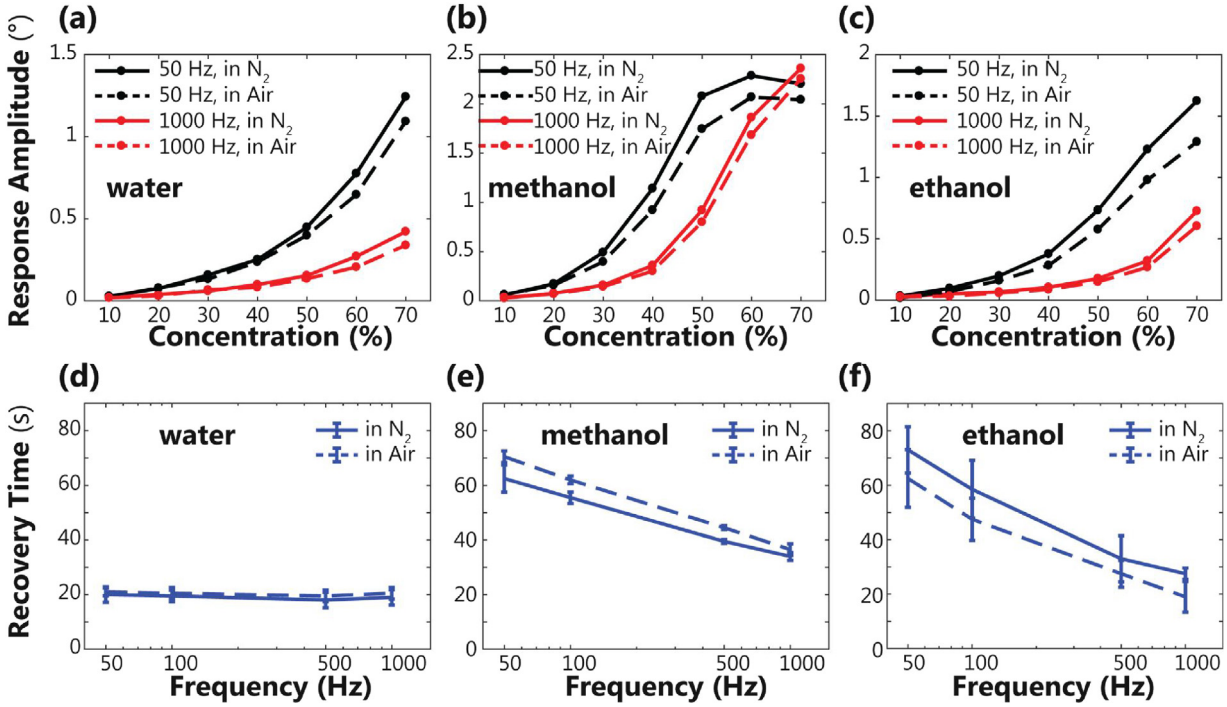

Fig. 6. Response amplitudes for (a) water, (b) methanol and (c) ethanol in the nitrogen and air environment at representative frequencies of 50 Hz and 1000 Hz. The 90% recovery time for (d) water, (e) methanol and (f) ethanol at different sensing frequencies with 90% gas vapor concentrations in nitrogen and air environment.

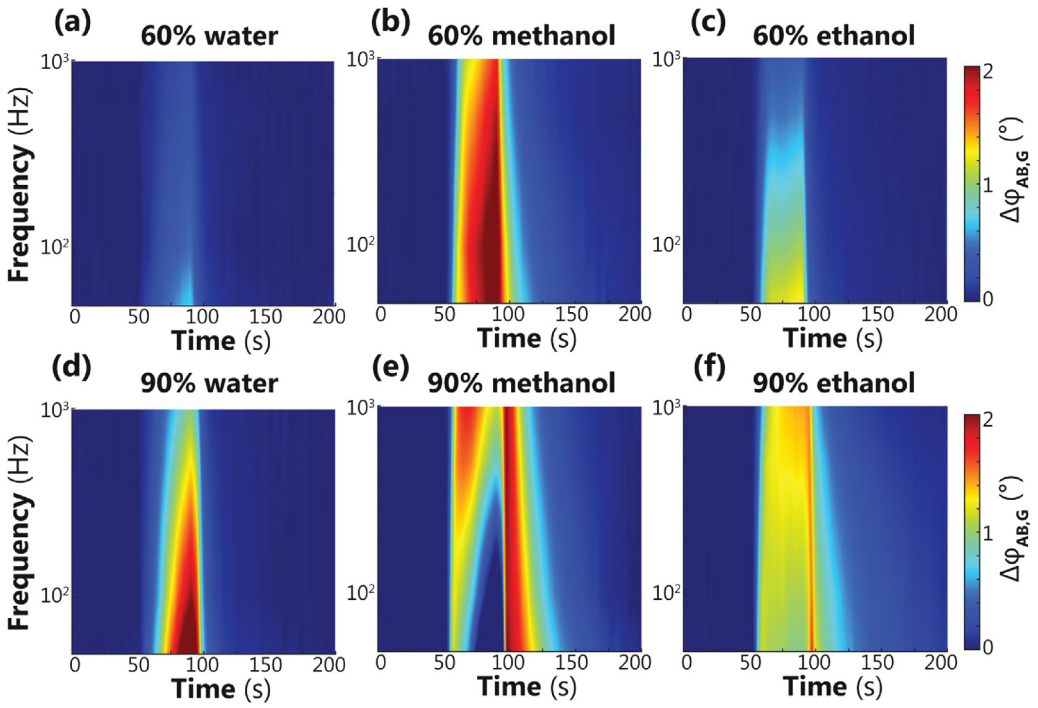

Fig. 7. The representative features of the frequency versus time phase lag spectra upon exposures to three chemical vapors (a–c) at their medium concentration (60%) and (d–f) at their high concentration (90%), respectively, as the vapor starts to enter the sensing system at 50 s and being purged with nitrogen at 90 s.

are difficult to be cleaned. This phenomenon can greatly damage the recovery speed as shown at the low frequency range while the recovery speed at high frequency (such as 1000 Hz) still maintains within 40 s in our testing results. Furthermore, it is potentially reasonable that different gas can induce different adsorption processes on the graphene surface such that the phase change results can be used as a feature to selectively sense the gas types. The slope of the phase change data could also correlate to the dynamic details of the adsorption process. The characteristics of phase change at different frequencies can be differentiated visually while specific machine learning or big data analyses tools could be applied in the future works for better and comprehensive identifications. The dynamic responses at higher frequency (over 1 kHz) are shown in Fig. S2 (Supplementary Information). The response amplitude decreases as the frequency increases from 1 kHz to 5 kHz which is in accordance with the trend observed in the previous lower frequency testing results. However, results from 5 kHz to 10 kHz are similar (or even show amplitude increases in the case of 80% methanol) implying possible deviations from the proposed simplified model at ultra-high frequency which needs further studies in the future.

AC sensing measurements under different humidity conditions from 20% to 60% RH were also performed by continuously feeding the water vapor into the chamber for 200 s before the inputs of target chemical vapors. All the experiments were carried at room temperature (24 °C). Dynamic responses of the phase lag changes are shown in Fig. 8 at exemplary frequencies of 50 Hz and 1000 Hz for ethanol under the 60% RH condition in air at room temperature. (other detail results in Fig. S3 for ethanol and Fig. S4 for methanol vapors). In general, the response amplitudes are enhanced as the RH level increases as shown in Fig. 9a for methanol vapors and Fig. 9b for ethanol vapors, as the result of the nonlinear response for each chemical vapor as illustrated in Fig. 6a, b, & c. The nonlinearity increases sharply when the concentration of humidity is greater than 40%. With accumulated water molecules as background, the incremental chemical vapor molecules will result in a larger response amplitude than those in the dry air condition. Interestingly, the phase change responses upon exposure to the RH background will mostly saturate within the first 50 s as shown in Fig. 8 and Fig. S3, such that one can clearly indicate the humidity level by comparing the sensing results with the initial reference sensing results in the dry air condition. In other words, the concentration of the target chemical vapor can be identified as the enhanced responses as the background RH level is first determined and extracted by the initial phase change results. Meanwhile, the 90% gas sensing recovery time increases as the RH level increases as shown in Fig. 9c for methanol and Fig. 9d for ethanol vapor with saturated concentrations, respectively, as the gas desorption process is suppressed by the background humidity when compared with the dry air condition.

4. Simulation and discussion

To explain the sensing results, we have developed a first-principle analytical model to describe the adsorption process of the gas molecule onto the graphene surface along with the charge transfer process [27]. The relationship between phase lag and the RC time constant of the model is derived. Specifically, this model uses an effective distance between the adsorbed gas molecule and graphene surface to determine the values of R and C and the phase lag associated with the distance between gas molecules and graphene surface reflects the adsorption strength.

In this model, each molecule-surface interaction pair is modeled as a DC voltage source (molecule) and an AC voltage source (sensing surface) connected by a series of charge transfer capacitor and charge transfer resistor (Fig. S5, Supplementary Information). The approaching process of the gas molecule onto the graphene surface is illustrated in Fig. 10a with the RC model shown in Fig. 10b. The carriers in the channel will flow back and forth under the modulation by the applied AC gate voltage [28]. The capacitor C has a phase lag between the channel resistance R_{AB} and the gate voltage V_g and it is defined as: $\varphi_{AB,g} \sim \varphi(\omega t)$. Analytically, an adsorption process with a large time constant would induce a smaller amplitude of phase lag in the RC model. The strength of adsorption process is distinguished by the parameter *d* which represents the distance

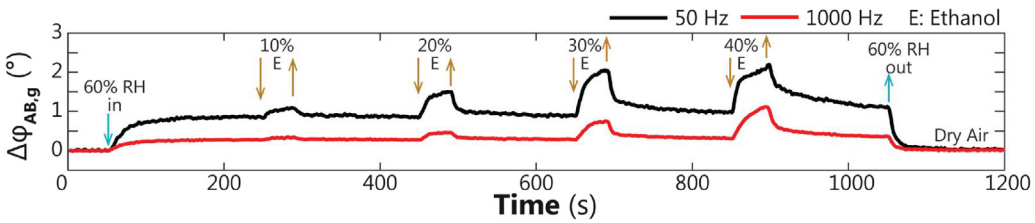

Fig. 8. Dynamic responses of phase lag changes at the exemplary frequencies of 50 Hz and 1000 Hz for ethanol vapors under 60% RH condition in air at room temperature (24 °C).

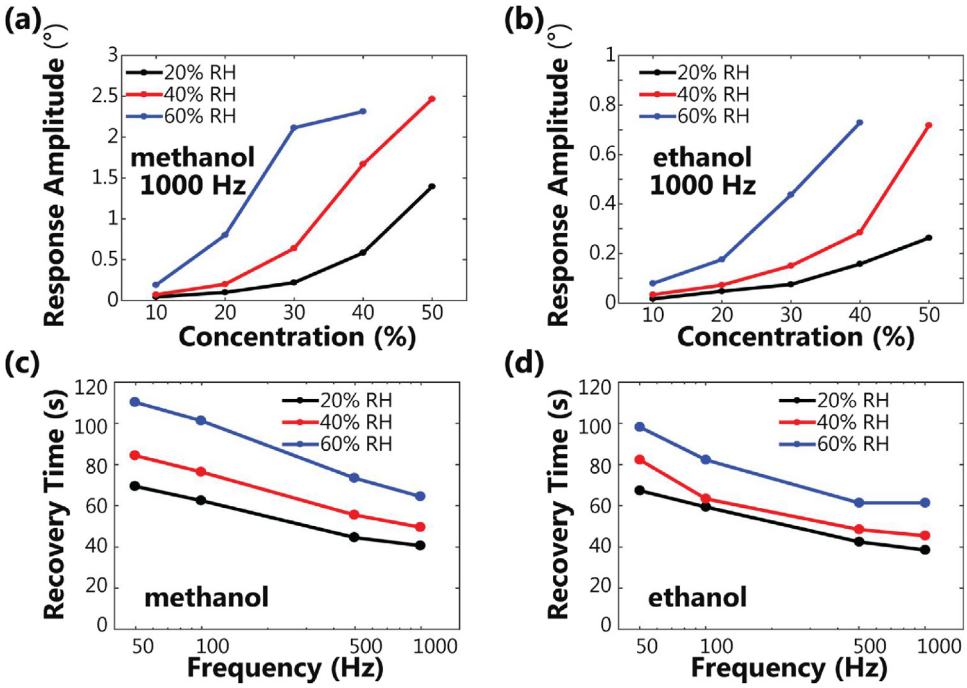

Fig. 9. Response amplitude for (a) methanol and (b) ethanol under different RH conditions in air at the frequency of 1000 Hz. The 90% recovery time for (c) methanol and (d) ethanol at different frequencies from 50 Hz to 1000 Hz with saturated gases under different RH conditions in air at room temperature (24 °C).

between the gas molecule and graphene surface. The resistance is modeled as a tunneling resistance $R \sim \exp(A\psi^{0.5}d)$ [29], where A is a constant with the value of 1.025 $A^{-1}eV^{-0.5}$, and ψ is the difference in electron affinity between the gas and graphene. The capacitance can be expressed as $C \sim \log(1 + r_{mo}/d)$ [30] using the infinite conducting plate model, where r_{mo} is the diameter of an individual gas molecule. Thus, the time constant of the charge transfer process between graphene and adsorbed gas molecules can be analyzed. For weakly adsorbed gases which have small time constants during the gas adsorption process, a large phase lag induced in R_{AB} is expected. This explains the fast recovery time of the phase responses for weakly adsorbed molecules. Specifically, the phase responses at high frequency are used to target/sense gas molecules in a short distance (as compared to those very close) to the graphene surface.

To simulate the transient response of phase response, we first calculate the induced phase change from molecules weighted by the sticking probability, then evaluate the integral responses of all adsorbed molecules by accumulating over the relevant range of $d < 30\ r_{mo}$. The profile of sticking probability of gas molecules on graphene surface agrees with the molecular number density distribution along the direction perpendicular to graphene given by molecular dynamics (MD) method analysis [31]. For simplicity, error functions were used to express the probability in the adsorption and desorption periods as $p_a(t) = 0.5 - 0.5\ \mathrm{erfc}(\alpha_a dt^{-0.5} r_{mo}^{-1})$ and $p_b(t) = 0.5\ \mathrm{erfc}(\alpha_d dt^{-0.5} r_{mo}^{-1})$, respectively, where t is time and $\alpha_{a,d}$ are the fitting constants. Two representative profiles of the sticking probability and their phase lag responses are plotted in Fig. 10c and Fig. 10d, respectively. Here, $d/r_{mo} = 2$ is used to represent the strongly adsorbed gases very close to the graphene surface which are expected to have strong adsorption and weak desorption properties, while $d/r_{mo} = 4$ (or larger) is used to represent the weakly adsorbed gases in a short distance away from the graphene surface which are expected to have slow adsorption and fast desorption properties. The representative responses of the sticking probability p in Fig. 10c show strong and fast responses during the adsorption process for gases close to the graphene surface ($d/r_{mo} = 2$) while during the desorption process, the gases at a short distance away to the graphene surface ($d/r_{mo} = 4$) have faster responses during the desorption process. Furthermore, the small dip in the phase lag testing results (such as those in Fig. 5b for high concentration methanol) in the adsorption process can be predicted by the model. Analytically, the initial protuberance of the phase lag results during the adsorption process for a short distance away from the graphene surface can be attributed to the large accumulations of gas molecules to result in the slow desorption process. This behavior is simulated numerically as shown in Fig. 10d for the case of $d/r_{mo} = 4$ curve. Nevertheless, the recovery speed for the $d/r_{mo} = 4$ curve is much faster than that for the case of the $d/r_{mo} = 2$ curve. These characteristics agree well with the experimental results in Fig. 7. However, it is noted that the proposed model only provides qualitative insights to explain the phase lag responses and advanced transport models should be developed

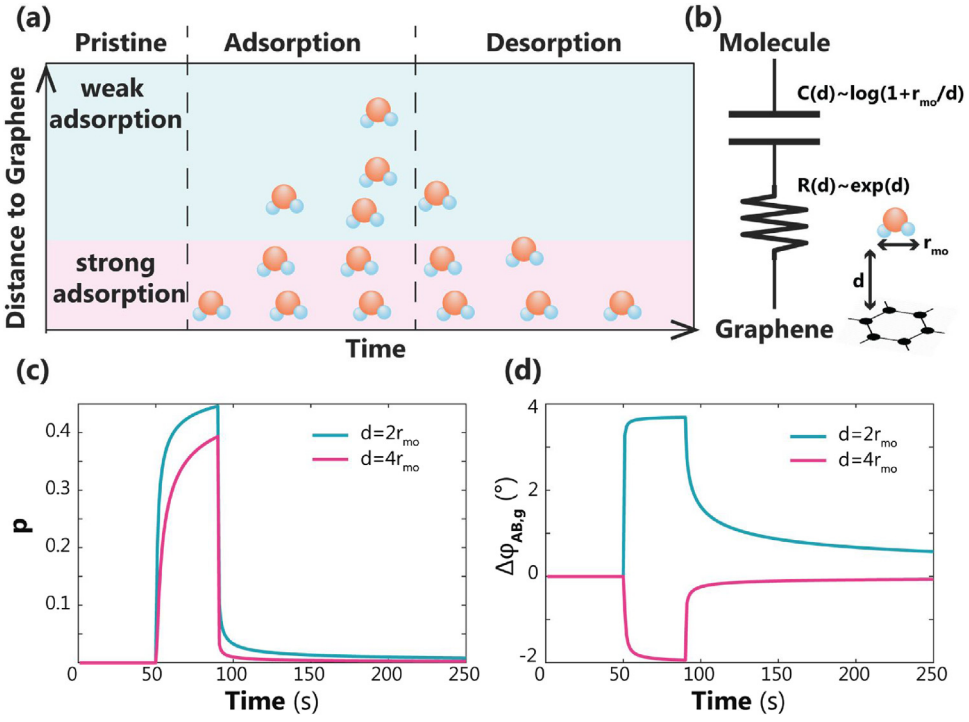

Fig. 10. (a) Schematic diagram illustrating the vapor adsorption and desorption process on the graphene surface – the AC sensing scheme is targeting weakly adsorbed gases a short distance away from the graphene surface while the DC sensing scheme is targeting molecules close to the graphene surface. (b) The RC model of the charge transfers pathway and process between adsorbed gas and graphene with a distance d away from the graphene surface. The resistance component scales up exponentially with d, while the capacitance scales down with d in a logarithmic manner. (c) The representative response of the sticking probability p and (d) the AC signal φ for the weakly adsorbed molecules ($d = 4\ r_{mo}$), and the strongly adsorbed molecules ($d = 2\ r_{mo}$).

with accurate properties for different gases to quantitatively fit the test results.

5. Conclusion

In summary, an AC phase sensing approach based on CVD-processed monolayer graphene FETs is utilized to sense chemical vapors. The recovery speed of the phase-based sensing approach is much faster than those of conventional DC resistance sensing schemes at room temperature. The superior performances of reversibility (low baseline drift) and fast recovery have been observed in different gas types (water, methanol, and ethanol) of different concentrations at room temperature. It is found that the recovery time can be shortened by using high input frequency sensing. The effects of relative humidity on methanol and ethanol gases has also been studied. Finally, an analytical model is developed to qualitatively explain the measurement results with good agreements.

Acknowledgements

This work was supported in part by the NSF grant (ECCS-1711227), Midea Group, the Philippine-California Advanced Research Institutes (PCARI) under the project of "Chemical and Environment – Portable Sensor Technologies (CE-PoST)", BSAC (Berkeley Sensor and Actuator Center, a NSF/Industry/University collaboration center), the National High Technology Research and Development Plan of China (2015AA043505), Shenzhen Fundamental Research Funds (JCYJ20150831192244849) and Shenzhen Technology Research Funds (JSGG20170414094227487). Huiliang Liu and Yao Chu gratefully acknowledge financial support from the China Scholarship Council. Xiaohao Wang, Zheng You, and Liwei Lin are core-principal investigators of the Tsinghua-Berkeley Shenzhen Institute (TBSI) and we acknowledge the funding support of TBSI.

Appendix A. Supplementary data

Supplementary data associated with this article can be found, in the online version, at https://doi.org/10.1016/j.snb.2018.01.244.

References

[1] A.K. Geim, K.S. Novoselov, The rise of graphene, Nat. Mater. 6 (2007) 183–191.
[2] G.R. Bhimanapati, Z. Lin, V. Meunier, Y. Jung, J. Cha, S. Das, et al., Recent advances in two-dimensional materials beyond graphene, ACS Nano 9 (2015) 11509–11539.
[3] K.S. Novoselov, V. Fal, L. Colombo, P. Gellert, M. Schwab, K. Kim, A roadmap for graphene, Nature 490 (2012) 192–200.
[4] F.K. Perkins, A.L. Friedman, E. Cobas, P. Campbell, G. Jernigan, B.T. Jonker, Chemical vapor sensing with monolayer MoS2, Nano Lett. 13 (2013) 668–673.
[5] B. Liu, L. Chen, G. Liu, A.N. Abbas, M. Fathi, C. Zhou, High-performance chemical sensing using schottky-contacted chemical vapor deposition grown monolayer MoS2 transistors, ACS Nano 8 (2014) 5304–5314.
[6] F. Schedin, A. Geim, S. Morozov, E. Hill, P. Blake, M. Katsnelson, et al., Detection of individual gas molecules adsorbed on graphene, Nat. Mater. 6 (2007) 652–655.
[7] E. Hwang, S. Adam, S.D. Sarma, Transport in chemically doped graphene in the presence of adsorbed molecules, Phys. Rev. B 76 (2007), 195421.
[8] W. Yuan, G. Shi, Graphene-based gas sensors, J. Mater. Chem. A 1 (2013) 10078–10091.
[9] H.J. Yoon, D.H. Jun, J.H. Yang, Z. Zhou, S.S. Yang, M.M.-C. Cheng, Carbon dioxide gas sensor using a graphene sheet, Sens. Actuators, B 157 (2011) 310–313.
[10] C.W. Chen, S.C. Hung, M.D. Yang, C.W. Yeh, C.H. Wu, G.C. Chi, et al., Oxygen sensors made by monolayer graphene under room temperature, Appl. Phys. Lett. 99 (2011), 243502.
[11] Y. Dan, Y. Lu, N.J. Kybert, Z. Luo, A.C. Johnson, Intrinsic response of graphene vapor sensors, Nano Lett. 9 (2009) 1472–1475.
[12] Y. Ren, C. Zhu, W. Cai, H. Li, H. Ji, I. Kholmanov, et al., Detection of sulfur dioxide gas with graphene field effect transistor, Appl. Phys. Lett. 100 (2012), 163114.
[13] H. Wang, Y. Wu, C. Cong, J. Shang, T. Yu, Hysteresis of electronic transport in graphene transistors, ACS Nano 4 (2010) 7221–7228.

[14] J.H. Chen, C. Jang, S. Xiao, M. Ishigami, M.S. Fuhrer, Intrinsic and extrinsic performance limits of graphene devices on SiO2, Nat. Nanotechnol. 3 (2008) 206–209.
[15] J. Martin, N. Akerman, G. Ulbricht, T. Lohmann, J.H. Smet, K. von Klitzing, et al., Observation of electron-hole puddles in graphene using a scanning single-electron transistor, Nat. Phys. 4 (2008) 144–148.
[16] I.-S. Kang, H.-M. So, G.-S. Bang, J.-H. Kwak, J.-O. Lee, C. Won Ahn, Recovery improvement of graphene-based gas sensors functionalized with nanoscale heterojunctions, Appl. Phys. Lett. 101 (2012), 123504.
[17] B. Kumar, K. Min, M. Bashirzadeh, A.B. Farimani, M.-H. Bae, D. Estrada, et al., The role of external defects in chemical sensing of graphene field-effect transistors, Nano Lett. 13 (2013) 1962–1968.
[18] K. Nemade, S. Waghuley, Role of defects concentration on optical and carbon dioxide gas sensing properties of Sb 2 O 3/graphene composites, Opt. Mater. 36 (2014) 712–716.
[19] G. Chen, T.M. Paronyan, A.R. Harutyunyan, Sub-ppt gas detection with pristine graphene, Appl. Phys. Lett. 101 (2012), 053119.
[20] R. Pearce, T. Iakimov, M. Andersson, L. Hultman, A.L. Spetz, R. Yakimova, Epitaxially grown graphene based gas sensors for ultra sensitive NO2 detection, Sens. Actuators, B 155 (2011) 451–455.
[21] G. Ko, H.-Y. Kim, J. Ahn, Y.-M. Park, K.-Y. Lee, J. Kim, Graphene-based nitrogen dioxide gas sensors, Curr. Appl. Phys. 10 (2010) 1002–1004.
[22] H. Choi, J.S. Choi, J.S. Kim, J.H. Choe, K.H. Chung, J.W. Shin, et al., Flexible and transparent gas molecule sensor integrated with sensing and heating graphene layers, Small 10 (2014) 3685–3691.
[23] G.S. Kulkarni, K. Reddy, Z. Zhong, X. Fan, Graphene nanoelectronic heterodyne sensor for rapid and sensitive vapour detection, Nat. Commun. 5 (2014), 4376.
[24] Y. Liu, J. Yu, Y. Cui, T. Hayasaka, H. Liu, X. Li, et al., An AC sensing scheme for minimal baseline drift and fast recovery on graphene FET gas sensor, in: 19th International Conference on Solid-State Sensors, Actuators and Microsystems (TRANSDUCERS), IEEE2017, 2017, pp. 230–233.
[25] J. Moser, A. Barreiro, A. Bachtold, Current-induced cleaning of graphene, Appl. Phys. Lett. 91 (2007), 163513.
[26] J.H. Chen, C. Jang, S. Adam, M.S. Fuhrer, E.D. Williams, M. Ishigami, Charged-impurity scattering in graphene, Nat. Phys. 4 (2008) 377–381.
[27] P.R. Bueno, F. Fabregat-Santiago, J.J. Davis, Elucidating capacitance and resistance terms in confined electroactive molecular layers, Anal. Chem. 85 (2012) 411–417.
[28] Y.-J. Yu, Y. Zhao, S. Ryu, L.E. Brus, K.S. Kim, P. Kim, Tuning the graphene work function by electric field effect, Nano Lett. 9 (2009) 3430–3434.
[29] G. Binnig, H. Rohrer, C. Gerber, E. Weibel, Surface studies by scanning tunneling microscopy, Phys. Rev. Lett. 49 (1982) 57.
[30] J.M. Crowley, Simple expressions for force and capacitance for a conductive sphere near a conductive wall, Proceedings of the ESA Annual Meeting on Electrostatics (2008), p. 1.
[31] C. Sun, B. Bai, Gas diffusion on graphene surfaces, Phys. Chem. Chem. Phys. 19 (2017) 3894–3902.

Biographies

Huiliang Liu received the B.S. degree in electronic engineering from Xiamen University, Xiamen, China, in 2012, and the M.S. degree in microelectronics from Tsinghua University, Beijing, China, in 2015. Previously, he worked on the RF MEMS varactor and UWB system for Body Area Network. He is currently working toward the Ph.D. degree at Tsinghua-Berkeley Shenzhen Institute, Tsinghua University, China. His current research is focused on the graphene chemical sensors.

Yumeng Liu received the B.Eng. degree in microelectronics from the Tsinghua University, Beijing, China, in 2012, and the M.Sc. degree in mechanical engineering from the University of California Berkeley, Berkeley, CA, USA, in 2014. He is currently a Ph.D. Candidate in the Department of Mechanical Engineering, University of California Berkeley. His research interests include modeling, condition monitoring, and modulation of FET gas sensors.

Yao Chu is a Ph.D. candidate at Sensors and Microsystems Laboratory, Tsinghua-Berkeley Shenzhen Institute. She received her B.S. degree (2014) in Mechanical Engineering from Shanghai Jiao Tong University, China and M.S. degree (2015) in Mechatronic and Robotic Systems from University of Pennsylvania, United States. Her research interests include Wearable Electronics and Paper-based Electronics.

Takeshi Hayasaka is a Ph.D. candidate and graduate student researcher working under Professor Liwei Lin in the Mechanical Engineering Department at University of California, Berkeley. He received his B.S. in Applied Physics from Hirosaki University, Hirosaki, Japan, in 2012, and his M.E. in Mechanical Engineering from Tohoku University, Sendai, Japan, in 2014. His research focuses on microelectromechanical systems (MEMS).

Nirav Joshi received his Ph.D. degree in Applied Physics from M.S. University of Baroda, India in 2012. Currently, he is working as a postdoctoral fellow at the University of California, Berkeley, USA. Over the years, he worked on high dielectric constant materials, polymer nanocomposite for capacitor and supercapacitor applications. His present research focuses on synthesis and characterization of oxide nanostructures and 2D material-based gas sensors.

Yong Cui received Ph.D. degree in Electrical Engineering from Beihang University, Beijing, China, in 2015.He is currently working as a Postdoctoral researcher of the Berkeley Sensor and actuator center at University of California, Berkeley, Berkeley, CA, USA. His research interests include micro/nano chemical sensors, and MEMS.

Xiaohao Wang received the bachelor's and Ph.D. degrees from Tsinghua University, in 1994 and 1999, respectively. From 1998–2001, he joined the Department of Precision Instrument, Tsinghua University, as an Assistant Professor He was promoted to an Associate Professor in 2001, Tsinghua University. From 2007–2008, he stayed with the Technical University of Berlin as a Visiting Scholar. In 2010, he became a Professor with the Department of Precision Instrument, Tsinghua University. He is currently Deputy Dean of Graduate School, Shenzhen, Tsinghua University. He is also serving as the Vice President of the Chinese Society of Micro-Nano Technology and the Vice Presidential Member of Test and Instrument Committee of Chinese Association of High Education. His research interests cover MEMS-based sensors, actuators, and ionizing sources and portable analytical instrument. He has authored over 200 technical papers and holds tens of patents in the area of MEMS and the portable instrumentation.

Zheng You received the B.S., M.S., and Ph.D. degrees in mechanical engineering from the Huazhong University of Science and Technology, Wuhan, China, in 1985, 1987, and 1990. Since 1994, he has been a Full Professor at Tsinghua University, in 2000 a Changjiang Scholar of the National Education Ministry, and in 2013 an academician of Chinese Academy of Engineering. He is Chairman of Chinese Society of Micronano Technology and Deputy Chairman of China Instrument and Control Society. His interest covers many research fields including space MEMS, biochemical and RF MEMS technology.

Liwei Lin received his Ph.D. degree from Mechanical Engineering Department, University of California at Berkeley in 1993. He is a Professor in the Mechanical Engineering Department, University of California at Berkeley, Co-Director of Berkeley Sensor and Actuator Center and co-deputy Director of the Tsinghua-Berkeley Shenzhen Institute. He has published more than 200 journal papers and 20 US patents. Dr. Lin is the North & South America editor for Sensors and Actuators A: Physical, and a Fellow of ASME. His current research interests include MEMS (Microelectromechanical Systems)/NEMS (Nanoelectromechanical Systems), nanotechnology, and design and manufacturing of microsensors and microactuators.